J Mater Sci (2007) 42:7162–7170
DOI 10.1007/s10853-007-1609-7

Anatase TiO_2 nanoparticles/carbon nanotubes nanofibers: preparation, characterization and photocatalytic properties

Guangjun Hu · Xiangfu Meng · Xiyan Feng · Yanfen Ding · Shimin Zhang · Mingshu Yang

Received: 27 November 2006 / Accepted: 12 February 2007 / Published online: 10 May 2007

Abstract In the present work, we report the preparation and photocatalytic properties of hybrid nanofibers/mats of anatase TiO_2 nanoparticles and multi-walled carbon nanotubes (MWNTs) using combined sol–gel and electrospinning techniques. Poly(vinyl pyrrolidone) is used as a base polymer in the electrospinning suspension to assist the formation of nanofibers and subsequently removed by calcination. The hybrid nanofibers are characterized using XRD, Raman spectra, FT-IR, XPS, SEM, TEM and N_2 adsorption measurements. The results show that MWNTs are encapsulated by in-situ formed anatase TiO_2 nanoparticles, with chemical bonding C–O–Ti between anatase TiO_2 nanoparticles and MWNTs. Hybrid nanofibrous mats with moderate content of MWNTs (mass ratio TiO_2:MWNTs = 100:20) exhibit enhanced adsorption ability and excellent photocatalytic activity. The composition, diameter and morphology of hybrid nanofibers can be tuned by varying sol–gel formulation, electrospinning parameter and post-treatment condition. TiO_2/MWNTs hybrid nanofiber and mats have promising applications in water purification and solar cell areas.

G. Hu · X. Meng · X. Feng · Y. Ding · S. Zhang · M. Yang (✉)
Beijing National Laboratory for Molecular Sciences, Key Laboratory of Engineering Plastics, Institute of Chemistry, Chinese Academy of Sciences, Beijing 100080, China
e-mail: yms@iccas.ac.cn

G. Hu · X. Meng · X. Feng
Graduate School of Chinese Academy of Sciences, Beijing 100039, China

Introduction

Due to its high refractive index, chemical reactivity and photochemical reactivity, titanium dioxide (TiO_2) is considered as one of the most important photocatalysts to solve environmental problems, especially in the purification of polluted water and air [1]. To enhance the photocatalytic efficiency and other properties of TiO_2, many efforts have been devoted to control the morphology and phase of TiO_2 [2, 3], and synthesize novel TiO_2 hybrid photocatalysts [4, 5].

Carbon nanotubes (CNTs) are molecular-scale tubes of graphitic carbons with exceptional electronic, mechanical and thermal properties [6], so it could be an ideal catalyst support material for TiO_2. Some works have reported the synthesis of TiO_2/CNTs nanoparticles [7–10], but there are still some tough obstacles to hinder their large-scale application. Such obstacles include difficulties to fix and reclaim these tiny nanoparticles in practical photocatalytic applications, and the potential toxicity of nanoparticles especially caused by their inhalation and penetration [11].

Electrospinning is a facile way to prepare nanofibers, and it can be used to convert nanoparticles into long nanofibers with the aid of a polymer base. In the present work, we demonstrate the preparation and photocatalytic properties of hybrid nanofibers and mats composed of anatase TiO_2 nanoparticles/MWNTs utilizing sol–gel and electrospinning techniques. MWNTs are encapsulated by the in-situ formed anatase TiO_2 nanoparticles. Chemical bonding between anatase TiO_2 and MWNTs nanoparticles is identified, and the mechanism for enhanced photocatalytic activity of hybrid nanofibrous mats is also discussed.

Experimental part

Materials and preparation

Pristine MWNTs were purchased from Shenzhen Nanotech Port Co., Ltd (Shenzhen, China). Typical specifications of MWNTs are: diameters of 10–20 nm, lengths of 5–15 μm. MWNTs were treated with concentrated HNO_3 (70%) and H_2SO_4 (98%) with a volume ratio of 2:1 at 95 ± 5 °C for 27 h. Carboxylic groups (–COOH) were identified by Fourier-transform infrared spectra (FT-IR). Carboxylated MWNTs were used because their enhanced dispersibility and negative charges favored the deposition of positive charged titanium complexes.

All the reagents except those specified were analytical grade and used without further purification. Poly (vinyl pyrrolidone) (PVP) was selected as the base polymer because of its good compatibility with both TiO_2 precursors [12] and CNTs [13]. Glacial acetic acid was added to control the hydrolysis and condensation of titanium alkoxide [14]. In a typical procedure, 4 mL ethanol suspension with carboxylated MWNTs was ultrasonicated for 3 h (200 W, 40 KHz). Then, 0.42 mL (0.00125 mol) tetra-*n*-butyl titanate (TBT, Beijing Chemical Reagent Company) and 1 mL glacial acetic acid were added in. After stirring for 15 min, the suspension was mixed with a solution of 0.77 g PVP (Aldrich, Mw ≈ 1,300,000) in 3 mL absolute ethanol, followed by magnetic stirring for 3 h. The resulted dark ink-like suspension was homogeneous and stable, exhibiting no phase separation for weeks. The mixture was loaded into a glass syringe equipped with a steel-made spinneret, whose inner diameter was about 0.4 mm. A DC voltage of 30 kV generated by a high-voltage supply was applied for electrospinning, and a piece of flat aluminum foil was placed 15 cm below the spinneret to collect nanofibers. The electrospinning was conducted in a ventilating cabinet. As-electrospun nanofibers were left in air for 24 h to hydrolyze TBT. Then, PVP was selectively removed from these nanofibers by calcining them at 500 °C for hours. For comparison, PVP, PVP/MWNTs and PVP/TiO_2 nanofibers were prepared by the same procedures, and their compositions are listed in Table 1. The calcined samples of as-electrospun nanofibers PVP/TiO_2, PVP/MWNTs, PVP/TiO_2/MWNTs (mass ratio PVP:TiO_2:MWNTs = 80:10:2), PVP/TiO_2/MWNTs (80:10:5) and PVP/TiO_2/MWNTs (80:10:10) are marked as TiF, NTF, Ti/NT2, Ti/NT5 and Ti/NT10, respectively. Commercial TiO_2 photocatalyst P25 (Degussa, ca. 80% anatase, 20% rutile) was also electrospun into mats, calcined under same conditions, and marked as P25F.

Characterization

Hitachi S-4300F field emission scanning electron microscope (SEM) and JEOL JEM-2010 transmission electron microscope (TEM) were used to observe the morphology of samples. Specimens of as-electrospun nanofibers for SEM and TEM studies were directly prepared by placing silicon wafers and carbon-coated copper grids on the aluminum foil during electrospinning. No coating was applied on all SEM specimens. Hybrid nanofibers for TEM observation were obtained by transferring the calcined nanofibers onto carbon-coated copper grids from the aluminum foils. Both bright-field images and selected area electron diffraction (SAED) patterns of nanofibers were recorded in TEM study.

X-ray diffraction (XRD) patterns were collected on a Rigaku D/max 2400 diffractometer using CuK_α radiation (λ = 0.15406 nm) at a scanning rate of 2 °/min. Raman spectra were taken on a Renishaw-2000 Raman spectrometer at a resolution of 2 cm^{-1} by using 514.5 nm line of an argon ion laser as excitation. IR spectra were recorded on a Perkin–Elmer System 2000 FT-IR spectrometer using KBr pellets method in the range of 370–4,000 cm^{-1}. Samples were irradiated under an IR lamp to eliminate adsorbed moisture prior to the experiments. X-ray photoelectron spectra (XPS) were recorded with ESCA Lab 220i-XL by using a monochromatized AlK_α (hv = 1486.6 eV) X-ray source. Brunauer–Emmett–Teller (BET) surface areas and porous

Table 1 Composition, average diameter, BET surface area and average pore size of nanofibers

	Mass ratio PVP:MWNTs:TiO_2	Average diameter of nanofibers (nm)		S^a_{BET} (m^2/g)	Pore size[b] (nm)
		As-electrospun	Calcined		
PVP	100:0:0	600 ± 215	–	–	–
PVP/MWNTs	90:10:0	390 ± 110	–	233.4	11.6
PVP/TiO_2	90:0:10	255 ± 140	70 ± 50	57.5	4.6
PVP/TiO_2/MWNTs	80:10:10	260 ± 70	65 ± 35	194.6	4.9

[a] N_2 adsorption experiments were carried out on the calcined nanofibers

[b] BJH desorption average pore diameter

structure were determined at 77 K by using a Micromeritics ASAP 2020 gas sorptometer. The samples were degassed at 300 °C for 24 h before measurements.

Photocatalytic activity

Azo compounds are widely used in industry; therefore the elimination of these compounds is becoming an increasingly important environmental problem. The azo compound, namely methyl orange (MO, Beijing Chemical Reagent Company), was chosen as the model pollutant in present work. Photodegradation of MO was evaluated under UV irradiation in an aqueous media. The initial concentration of MO was set as 10 mg/L. The amount of photocatalysts including TiO_2 and MWNTs was kept at 0.25 g/L. Before UV irradiation, the suspension containing photocatalyst nanofibrous mats and MO was deposited overnight to establish adsorption–desorption equilibrium. Then, the suspension was irradiated under a UV lamp (wavelength = 300 nm). The concentration of MO was traced by UV–vis spectroscopy (Shimadzu UV-1601PC). Each sample was recorded in full spectrum (200–800 nm), and the absorbance at characteristic band 463 nm was taken to determine MO concentration using a calibration curve of absorbance vs. concentration. Repetition tests were made to ensure the data reliability.

Results and discussion

XRD, XPS, IR and Raman spectroscopy

XRD patterns of nanofibers are displayed in Fig. 1. For as-electrospun nanofibers (Fig. 1a), no major peaks can be attributed to crystalline TiO_2, while the peak at about 25.5° in PVP/MWNTs and PVP/TiO_2/MWNTs is assigned to MWNTs. These results suggest that crystalline TiO_2 nanoparticles are not yet formed. After removing PVP by calcination, the characteristic peaks of TiO_2 including both anatase and rutile phases [3] emerged in the residual TiF nanofibers and TiO_2/MWNTs hybrid nanofibers (Fig. 1b), indicating that crystalline TiO_2 nanoparticles are formed mainly in the calcination stage. Crystallite size (D) and anatase fraction (X_A) of crystalline TiO_2 can be calculated using the equations deduced by Scherrer, Spurr and Myers [15], respectively. For neat TiF nanofibers, D and X_A of crystalline TiO_2 are 8 nm and 0.98, respectively. Using a thermodynamic model, Barnard et al. found that there was an intrinsic relationship between the size and phase of TiO_2: macroscopically anatase phase was metastable, and rutile phase was stable, but when particle size was under ~20 nm, this situation was reversed [16]. Our experimental results agree well with their modeling analysis. For TiO_2/MWNTs hybrid nanofibers, because the [101] reflection of anatase (2θ = 25.3°) overlaps with the largest reflection of MWNTs (2θ = 25.5°), it is hard to deduce the crystallite size and mass fraction of anatase within. However, from the intensity of [110] peak (2θ = 27.4°) of rutile TiO_2, it can be concluded that the mass fraction of rutile TiO_2 in TiO_2/MWNTs hybrid nanofibers should be very low.

Raman spectra of carboxylated MWNTs, neat TiF nanofibers and Ti/NT10 hybrid nanofibers are presented in Fig. 2a. The intensity ratio I_D/I_G of D-band (disordered carbon induced) over G-band (graphite carbon related) of MWNTs [17] changes from 1.1 of carboxylated MWNTs to 0.8 of Ti/NT10 hybrid nanofibers. This implies that improved graphite structure of MWNTs has been developed in the stage of calcination, which is in favor of enhancing the electrical and thermal conductivity of MWNTs. Characteristic bands at 396.4, 514.1 and 635.7 cm^{-1} in TiF nanofibers correspond to the B_{1g}, $A_{1g} + B_{2g}$ and E_g modes of anatase, respectively [18]. After hybridization with MWNTs, Raman band corresponding to E_g mode is shifted to lower energy, indicating a decrease in crystal lattice vibration energy and therefore a decrease in the crystallinity of anatase. And the line width broadens, suggesting a broader size distribution of anatase TiO_2 nanoparticles.

IR spectra of carboxylated MWNTs, neat TiF nanofibers and Ti/NT10 hybrid nanofibers are presented in Fig. 2b. For carboxylated MWNTs, the band at 1,574 cm^{-1} is assigned to C=C stretching originated from the inherent

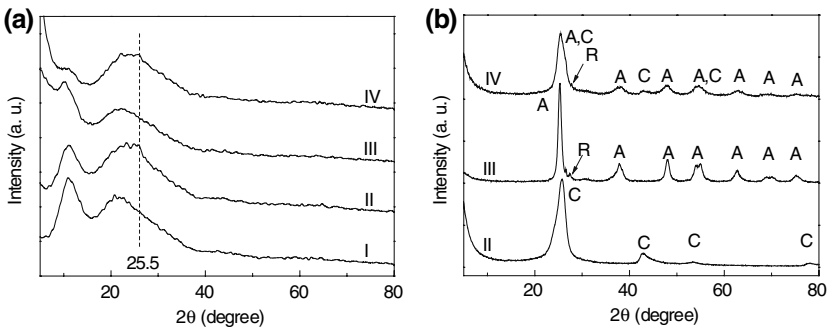

Fig. 1 XRD patterns of (**a**) as-electrospun nanofibers and (**b**) calcined nanofibers. I, PVP; II, PVP/MWNTs; III, PVP/TiO_2 and IV, PVP/TiO_2/MWNTs (mass ratio 80:10:10). The letters A, R and C stand for anatase, rutile TiO_2 and MWNTs, respectively (For the convenience of view, these curves are shifted in the vertical direction.)

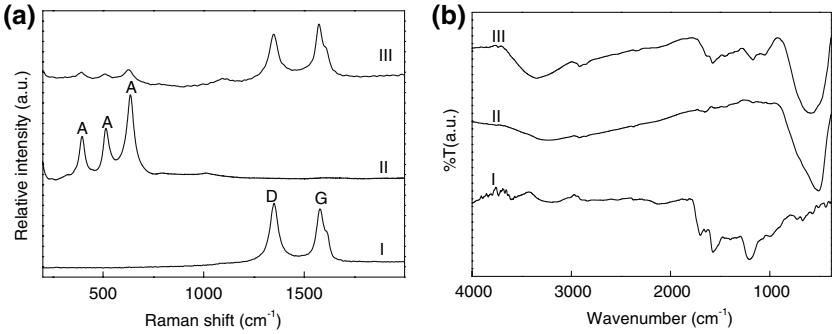

Fig. 2 Raman (**a**) and IR (**b**) spectra of (I) carboxylated MWNTs, (II) TiF nanofibers and (III) Ti/NT10 hybrid nanofibers. The letters A, D and G in (**a**) stand for anatase TiO_2, D-band and G-band of MWNTs, respectively

structure of MWNTs, and the bands at 1,704 and 1,210 cm^{-1} correspond to C=O, C–O stretching of carboxyl groups [19], respectively. For TiF nanofibers, the band peaked at 509 cm^{-1} corresponds to Ti–O–Ti vibration of anatase. As for Ti/NT10 hybrid nanofibers, the band at 1,576 cm^{-1} indicates the presence of MWNTs, and the band at 1,171 cm^{-1} suggests the presence of C–O bond; while the broad peak at 587 cm^{-1} is much plumper than the corresponding peak in TiF nanofibers and shifts towards high wavenumber. In fact, this peak can be looked as a combination of Ti–O–Ti vibration (509 cm^{-1}) and Ti–O–C vibration [20] (around 620 cm^{-1}, based on IR spectrum of TBT). The presence of Ti–O–C bonding indicates that TiO_2 nanoparticles are chemically bonded with MWNTs in hybrid nanofibers. Moreover, the band at 3,350 cm^{-1} is more prominent in Ti/NT10 hybrid nanofibers than that of TiF nanofibers, indicating that there are more hydroxyl groups in the hybrid nanofibers. More hydroxyl groups result in more $^{\bullet}OH$ radicals, which could enhance the photocatalytic activity of TiO_2.

XPS spectra of carboxylated MWNTs and Ti/NT10 hybrid nanofibers are presented in Fig. 3. There is a large

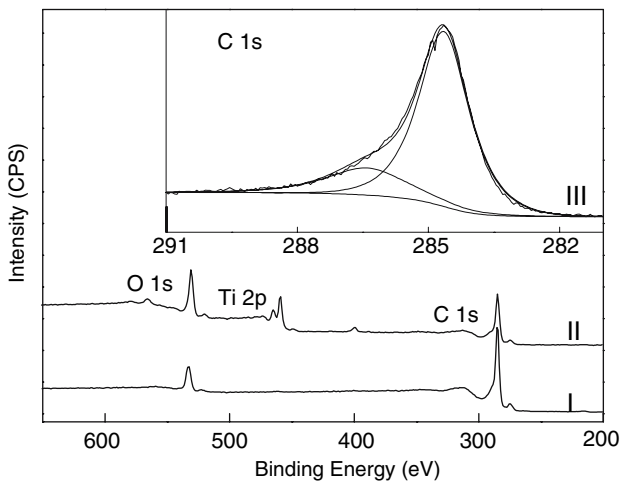

Fig. 3 XPS spectra of (I) carboxylated MWNTs, (II) Ti/NT10 nanofibers and (III) C 1s high-resolution for Ti/NT10 nanofibers

quantity of oxygen in carboxylated MWNTs, which belongs to carboxyl groups. In the fit of high-resolution spectrum C 1s of Ti/NT10 hybrid nanofibers, the peak at 284.6 eV is assigned to sp^2 C=C corresponding to the bulk structure of MWNTs, and the peak at 286.4 eV is assigned to carbon in C–O bond [21].

Microscopic characterization

Continuous nanofibers of different compositions have been successfully obtained without beads, which were unambiguously reflected from microscopic observations. As listed in Table 1, average diameter of as-electrospun nanofibers measured from microscopic images decreases noticeably from PVP (600 ± 215 nm) to PVP/MWNTs (390 ± 110 nm), PVP/TiO_2 (255 ± 140 nm) and PVP/TiO_2/MWNTs (260 ± 70 nm) with the addition of MWNTs and TiO_2 precursor. The reduction of average diameter with the addition of MWNTs and TiO_2 precursor can be attributed to the increased conductivity and electrospinning speed.

TEM images of as-electrospun PVP/MWNTs and PVP/TiO_2/MWNTs composite nanofibers are displayed in Fig. 4. For PVP/MWNTs composite nanofibers (Fig. 4a), although MWNTs account for 10 wt.% of content, they are successfully embedded and dispersed in nanofibers, and most MWNTs are oriented along the nanofiber axis due to the strong stretching effect of electric field in electrospinning process. Carboxylic acid groups on MWNTs are able to form intermolecular hydrogen bonds with polar solvents such as water and alcohols, which improves the dispersion of MWNTs. For PVP/TiO_2/MWNTs composite nanofibers (Fig. 4b), the entanglement of MWNTs is further reduced with the presence of TiO_2 precursors, and MWNTs are more homogeneously dispersed. This confirms a successful dissociation of MWNTs bundles in TiO_2 sol. SAED pattern reveals no diffraction rings related to crystalline TiO_2, which is consistent with XRD results. In the sol–gel process, carboxylated MWNTs are ''soluble'' in alcohol with the aid of hydrogen bond. TBT esters hydrolyze and generate Ti(IV) complexes, $[Ti(OH)(H_2O)_5]^{3+}$ [22]. These

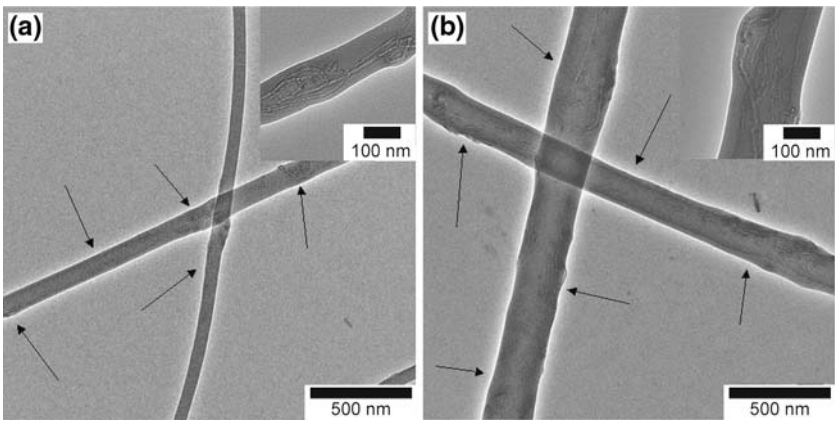

Fig. 4 Typical TEM images of as-eletrospun composite nanofibers in low and high magnifications. (**a**) PVP/MWNTs, (**b**) PVP/TiO_2/MWNTs (mass ratio 80:10:10). The arrows indicate MWNTs embedded in PVP matrix

cationic complexes preferably nucleate on the sidewalls of carboxylated MWNTs through esterification and electrostatic attraction. Simultaneously, complex ions nearby could react with each other through oxolation. Thus, TiO_2 nuclei adhere to MWNTs surfaces by C–O–Ti bond, and prevent the dissociated MWNTs from reaggregation.

The calcination treatment transforms as-electrospun composite nanofibers into NTF, TiF and Ti/NT nanofibers. The morphology of the resultant MWNTs fibers (NTF) changes dramatically compared with that of PVP/MWNTs composite nanofibers (Fig. 5a, b). The dimension of calcined NTF fibers was broadened very much and even

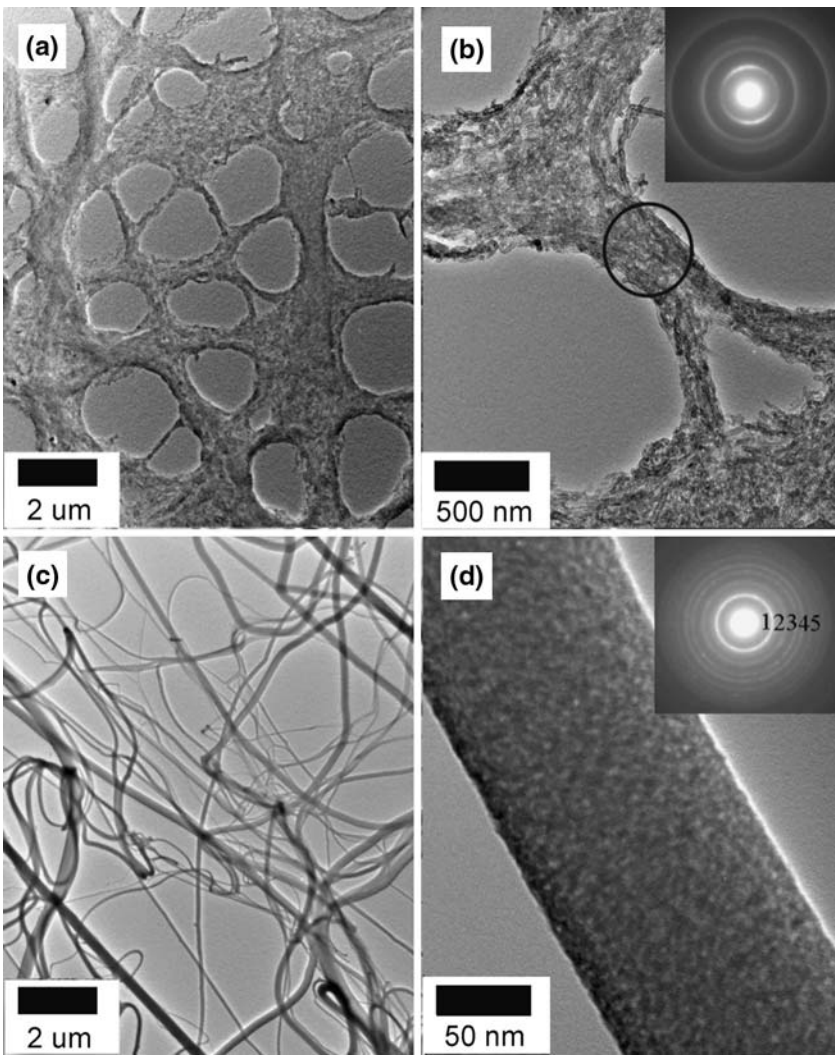

Fig. 5 Typical TEM images of MWNTs fibers [(**a**) and (**b**)] and TiF nanofibers [(**c**) and (**d**)] in low and high magnifications. They were obtained by calcining PVP/MWNTs and PVP/TiO_2 composite nanofibers at 500 °C for 90 min, respectively. The inset images in (**b**) and (**d**) are the corresponding SAED patterns

losing the fiber form because neighboring nanofibers merged together during the calcination stage. Meanwhile the alignment of MWNTs along fiber axis was apparently demonstrated in high magnification images, and also clearly reflected from SAED patterns. In the calcination stage of PVP/MWNTs composite nanofibers, PVP melted and burned, and adjacent nanofibers merged to reduce surface energy. After PVP was consumed, adjoining MWNTs in neighboring nanofibers welded into huge MWNTs bundles probably due to van der Waals forces and the driving force to reduce surface energy. The morphology of TiF nanofibers is quite different from NTF (Fig. 5c, d). The average diameter of TiF nanofibers was just about a quarter of that of the as-electrospun PVP/TiO_2 composite nanofibers (Table 1). In the calcination stage of PVP/TiO_2 composite nanofibers, PVP was burned out, and TiO_2 nanoparticles formed and interconnected by stepwise dehydration. This process led to a quick shrinkage of nanofibers; thus fine individual TiF nanofibers are formed. High magnification image indicates that the diameter of TiO_2 nanoparticles is just about 6 nm, which is consistent with the calculation result from Scherrer equation. The diffraction rings in inset SAED pattern are indexed as (1) [101], (2) [103] + [004] + [112], (3) [200], (4) [105] + [211] and (5) [213] + [204] for anatase [23].

Figure 6 presents typical TEM bright-field images and SAED patterns of Ti/NT10 hybrid nanofibers, which are obtained by calcining PVP/TiO_2/MWNTs (80:10:10) composite nanofibers at 500 °C for 45 and 90 min, respectively. Similar to TiF, these hybrid nanofibers are also thin, and the average diameter is about a quarter of that of the as-electrospun Ti/NT10 composite nanofibers (Table 1). Although MWNTs accounts for half mass of calcined samples, they are encapsulated by TiO_2 nanoparticles. MWNTs act as core, and TiO_2 nanoparticles that are chemically bonded on MWNTs behave as shell. The presence of MWNTs also makes the surface of hybrid nanofibers rougher in comparison with that of neat TiF

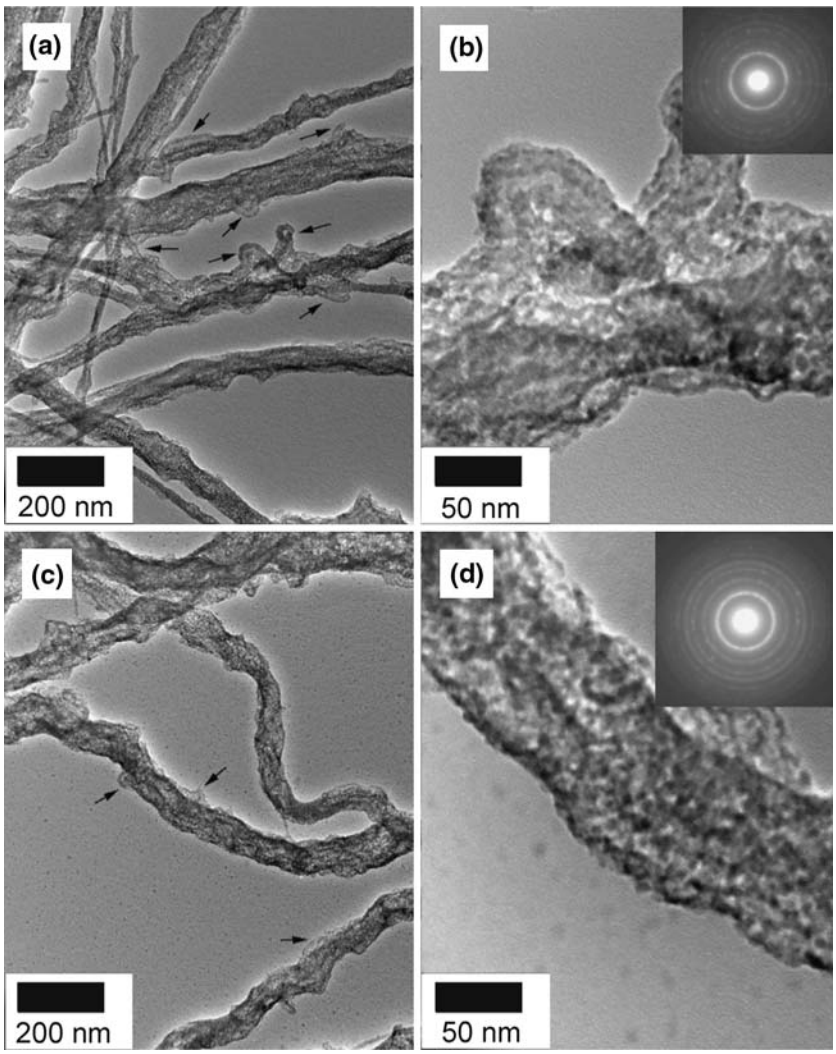

Fig. 6 Typical TEM images of Ti/NT10 hybrid nanofibers calcined for different time in low and high magnifications. The insets in (**b**) and (**d**) are the corresponding SAED patterns. (**a**) and (**b**) Ti/NT10 composite nanofibers calcined at 500 °C for 45 min; (**c**) and (**d**) Ti/NT10 composite nanofibers calcined at 500 °C for 90 min. The arrows in **a** and **c** indicate protruded MWNTs in hybrid nanofibers

nanofibers. As revealed in high magnification images, individual protruded MWNTs are covered by TiO_2 nanoparticles with diameters in few nanometers. The diffraction rings in SAED patterns in Fig. 6b, d are mainly assigned to anatase TiO_2. The comparison between these two patterns shows that diffraction rings are strengthened with longer calcination time. The quick shrinking process of forming TiO_2 nanoparticles prevents the merging of adjacent nanofibers, which predominates the calcination stage of PVP/MWNTs composite nanofibers. After PVP consumed, much thinner separated Ti/NT10 hybrid nanofibers forms. Moreover, the encapsulation of anatase TiO_2 nanoparticles prevents MWNTs from reaggregation due to the strong C–O–Ti chemical bonding.

N_2 adsorption study and photocatalytic activity evaluation

N_2 adsorption–desorption isotherms and pore size distribution plots of carboxylated MWNTs, TiF nanofibers and Ti/NT10 hybrid nanofibers are presented in Fig. 7. The values of BET surface area and average pore size are listed in Table 1. For N_2 adsorption and desorption isotherms, all of them are typical type IV adsorption isotherms with hysteresis, which are characteristic of mesoporous materials [24]. The pore size of TiF nanofibers is narrowly distributed and changes in the range of 1.5–12 nm. The presence of MWNTs broadens the pore size distribution, but just slightly influences the average pore size, consistent with Raman analysis. BET surface area of TiF nanofibers is 57.5 m^2/g, while the hybridization with MWNTs greatly increases it to 194.6 m^2/g (Ti/NT10).

Before photodegradation experiments, MO aqueous solutions with different photocatalyst nanofibrous mats were deposited in dark overnight to reach adsorption–desorption equilibrium. Ti/NT2, Ti/NT5 and Ti/NT10 nanofibrous mats revealed increased adsorption capabilities in comparison with TiF nanofibrous mat. The increased adsorption capability with increased amount of MWNTs was largely due to the increased surface area. However, Ti/NT10 nanofibrous mat did not exhibit apparent photocatalytic activity under UV irradiation. The lower photocatalytic activities of photocatalysts with high content of MWNTs can be explained by that excess MWNTs shield UV light from TiO_2 nanoparticles, thus photocatalyst cannot exhibit photocatalytic activity. UV–vis spectra evolution of MO with photocatalyst Ti/NT2 nanofibrous mat versus UV irradiation time is shown in Fig. 8.

Photodegradation of MO under UV irradiation follows pseudo-first-order kinetics with the concentration of MO (Fig. 9a). This relation can be described into the following relation:

$$\ln\left(\frac{C_0}{C}\right) = K_a t, \tag{1}$$

where C_0 is the concentration when UV irradiation starts, and K_a is the apparent photodegradation rate constant. K_a value is calculated from the slope of $\ln(C_0/C)$ vs. t. Based on the same mass of efficient photocatalytic content TiO_2, K_a values of photocatalysts are plotted with columns in Fig. 9b. Ti/NT2 nanofibrous mats show excellent photocatalytic activity in comparison with TiF or P25F nanofibrous mats.

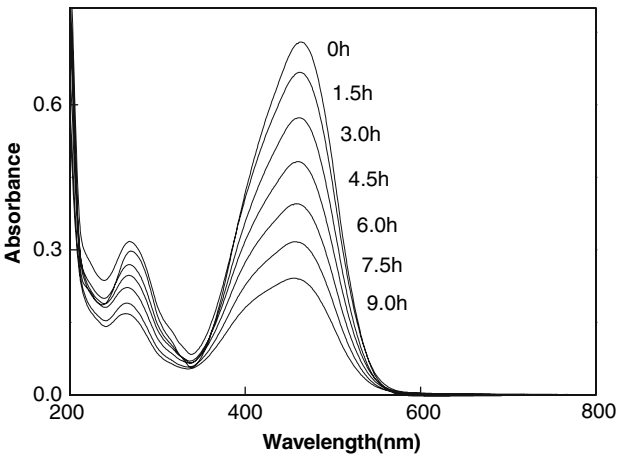

Fig. 8 UV–vis spectra evolution of MO with photocatalyst Ti/NT2 nanofibrous mat vs. UV irradiation time

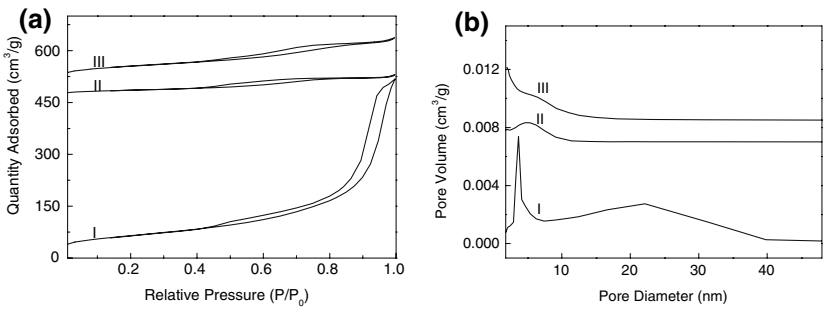

Fig. 7 N_2 adsorption and desorption isotherms and pore size distribution plot of (I) carboxylated MWNTs, (II) TiF nanofibers and (III) Ti/NT10 hybrid nanofibers

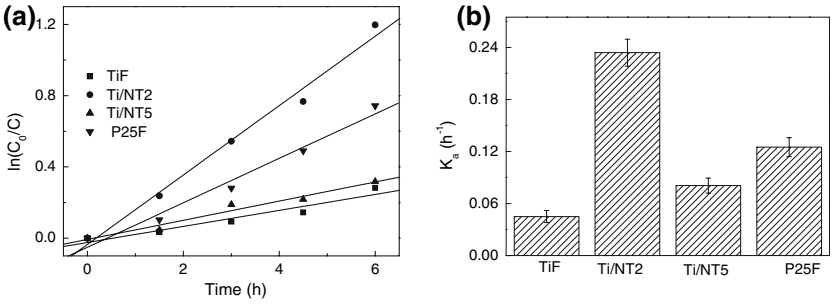

Fig. 9 (**a**) Degradation kinetics of MO with different photocatalyst nanofibrous mats vs. irradiation time; (**b**) photocatalytic activity comparison of different photocatalyst nanofibrous mats based on same mass of TiO_2. Error bars means one standard deviation from the mean values

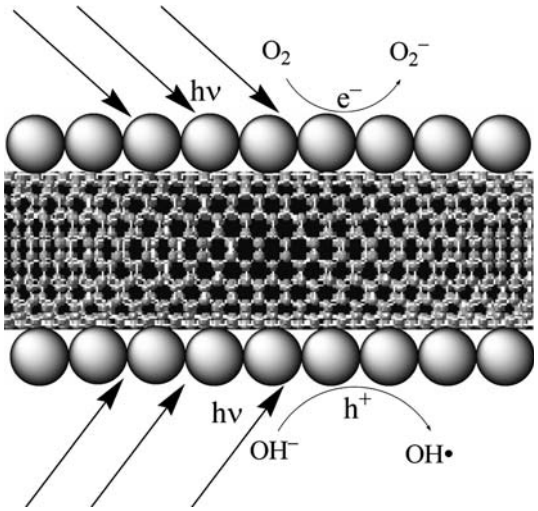

Fig. 10 Schematic illustration of photocatalytic mechanism of TiO_2/MWNTs hybrid nanofibers

A lot of photodegradation reactions follow the mechanism: organic compounds are adsorbed on the surface of photocatalyst, and oxidized by highly reactive radicals produced thereon [25]. In the TiO_2/MWNTs hybrid nanofibers with moderate content of MWNTs, in-situ formed TiO_2 nanoparticles encapsulated MWNTs, and bonded with MWNTs by C–O–Ti bonding. MWNTs increased the surface area and adsorption ability of hybrid photocatalysts, and decreased the agglomeration of TiO_2 nanoparticles. The strong interaction between anatase TiO_2 nanoparticles and MWNTs led to synergic effects (Fig. 10). During photocatalysis process, large quantities of highly reactive radicals, including superoxide radical ion $O_2^{\bullet-}$ and hydroxyl radical $^{\bullet}OH$, are generated on anatase TiO_2 nanoparticle surface, and electrons (e^-) and positive charged holes (h^+) are also massively formed [9, 10]. Without MWNTs, these opposite charges could recombine, form e^-/h^+ pairs and diminish the number of radicals. The presence of conductive MWNTs can quickly transport these charges, minimize the chance of e^-/h^+ pair recombination, and hence enhance the photocatalytic efficiency of anatase TiO_2. Besides, more hydroxyl groups in TiO_2/MWNTs hybrid nanofibers (based on IR results) also contribute to the improvement.

Conclusion

In summary, we prepared hybrid nanofibers and mats of anatase TiO_2 nanoparticles/MWNTs utilizing combined sol–gel and electrospinning techniques, and found that these hybrid materials have exhibited enhanced photocatalytic properties. These hybrid nanofibers have been investigated using XRD, Raman spectra, FT-IR, XPS, SEM, TEM and N_2 adsorption measurements. The results show that MWNTs are encapsulated by in-situ formed anatase TiO_2 nanoparticles, with chemical bonding C–O–Ti between anatase TiO_2 nanoparticles and MWNTs.

With moderate content of MWNTs (mass ratio TiO_2:MWNTs = 100:20), hybrid nanofibrous mats exhibit excellent photocatalytic activity. The improvement of photocatalysis efficiency probably comes from the following factors. First, due to the presence of strong chemical bonding between anatase TiO_2 nanoparticles and MWNTs, moderate content of MWNTs decreases the agglomeration of TiO_2 nanoparticles, induces small size anatase TiO_2 nanoparticles, and increases the surface area and adsorption ability of hybrid photocatalysts. Second, MWNTs can quickly transport charges generated in photocatalysis process, minimize the chance of e^-/h^+ pair recombination. Thirdly, more hydroxyl groups in hybrid materials may also contribute to photocatalysis activity.

The present approach, which combines sol–gel and electrospinning techniques, is flexible in preparing TiO_2/CNTs hybrid nanofibers. The composition, diameter, and morphology of hybrid nanofibers can be tuned by varying sol–gel formulation, electrospinning parameter and post treatment condition. This approach is controllable, facile and environmentally friendly. These nanofibrous mats are easy to be fixed and reclaimed in water purification applications that benefit the usage and recovery of photocatalyst. TiO_2/CNTs hybrid nanofibers and mats have potential applications not only in polluted water treatment but also in other areas such as sensors and solar cells.

Acknowledgments Financial support for this study was provided by National Natural Science Foundation of China (50473054 and 50533070).

References

1. Fujishima A, Rao TN, Tryk DA (2000) J Photochem Photobiol C 1:1
2. Zhang HZ, Finnegan M, Banfield JF (2001) Nano Lett 1:81
3. Wang W, Gu BH, Liang LY, Hamilton WA, Wesolowski DJ (2004) J Phys Chem B 108:14789
4. Tryba B, Morawski AW, Inagaki M (2003) Appl Catal B 46:203
5. Long RQ, Chang MT, Yang RT (2001) Appl Catal B 33:97
6. Dai H (2002) Acc Chem Res 35:1035
7. Huang Q, Gao L (2003) J Mater Chem 13:1517
8. Lee SW, Sigmund WM (2003) Chem Commun 6:780
9. Yu Y, Yu JC, Yu J, Kwok Y, Che Y, Zhao J, Ding L, Ge WK, Wong PK (2005) Appl Catal A 289:186
10. Wang WD, Serp P, Kalck P, Faria JL (2005) J Mol Catal A Chem 235:194
11. Lam CW, James JT, McCluskey R, Hunter RL (2004) Toxicol Sci 77:126
12. Li D, Xia Y (2003) Nano Lett 3:555
13. O'Connell MJ, Boul P, Ericson LM, Huffman C, Wang YH, Haroz E, Kuper C, Tour J, Ausman KD, Smalley RE (2001) Chem Phys Lett 342:265
14. Gopal M, Moberly C, De Jonghe LC (1997) J Mater Sci 32:6001
15. Spurr RA, Meyers H (1957) Anal Chem 29:760
16. Barnard AS, Curtiss LA (2005) Nano Lett 5:1261
17. Okpalugo TIT, Papakonstantinou P, Murphy H, Mclaughlin J, Brown NMD (2005) Carbon 43:2951
18. Wilson GJ, Will GD, Frost RL, Montgomery SA (2002) J Mater Chem 12:1787
19. Zhang J, Zou HL, Qing Q, Yang YL, Li QW, Liu ZF, Guo XY, Du ZL (2003) J Phys Chem B 107:3712
20. Zhu YF, Zhang L, Gao C, Cao LL (2000) J Mater Sci 35:4049
21. Ramanathan T, Fisher FT, Ruoff RS, Brinson LC (2005) Chem Mater 17:1290
22. Henry M, Jolivert JP, Livage J (1992) In: Reisfeld R, Jorgensen CK (eds) Aqueous chemistry of metal cations, hydrolysis, condensation, and complexation. Springer-Verlag, Berlin, p 155
23. Sasaki T, Nakano S, Yamauchi S, Watanabe M (1997) Chem Mater 9:602
24. Schmidt R, Hansen EW, StiScker M, Akporiaye D, Ellestad OH (1995) J Am Chem Soc 117:4049
25. Ollis DF, Hsiao CY, Budiman L, Lee CL (1984) J Catal 88:89